

ACCEPTED MANUSCRIPT

## DUV fluorescence bioimaging study of the interaction of partially reduced graphene oxide and liver cancer cells

To cite this article before publication: Radovan J Dojcilovic *et al* 2018 *2D Mater.* in press <https://doi.org/10.1088/2053-1583/aad72b>

### Manuscript version: Accepted Manuscript

Accepted Manuscript is “the version of the article accepted for publication including all changes made as a result of the peer review process, and which may also include the addition to the article by IOP Publishing of a header, an article ID, a cover sheet and/or an ‘Accepted Manuscript’ watermark, but excluding any other editing, typesetting or other changes made by IOP Publishing and/or its licensors”

This Accepted Manuscript is © 2018 IOP Publishing Ltd.

During the embargo period (the 12 month period from the publication of the Version of Record of this article), the Accepted Manuscript is fully protected by copyright and cannot be reused or reposted elsewhere.

As the Version of Record of this article is going to be / has been published on a subscription basis, this Accepted Manuscript is available for reuse under a CC BY-NC-ND 3.0 licence after the 12 month embargo period.

After the embargo period, everyone is permitted to use copy and redistribute this article for non-commercial purposes only, provided that they adhere to all the terms of the licence <https://creativecommons.org/licenses/by-nc-nd/3.0>

Although reasonable endeavours have been taken to obtain all necessary permissions from third parties to include their copyrighted content within this article, their full citation and copyright line may not be present in this Accepted Manuscript version. Before using any content from this article, please refer to the Version of Record on IOPscience once published for full citation and copyright details, as permissions will likely be required. All third party content is fully copyright protected, unless specifically stated otherwise in the figure caption in the Version of Record.

View the [article online](#) for updates and enhancements.

# DUV fluorescence bioimaging study of the interaction of partially reduced graphene oxide and liver cancer cells

Radovan Dojčilović<sup>a,b</sup>, Jelena D. Pajović<sup>c,d</sup>, Dušan K. Božanić<sup>a,e</sup>, Nataša Jović<sup>a</sup>, Vera P. Pavlović<sup>f</sup>, Vladimir B. Pavlović<sup>g,h</sup>, Lea Lenhardt Acković<sup>a</sup>, Ivana Zeković<sup>a</sup>, Miroslav Dramićanin<sup>a</sup>, Slavka Kaščaková<sup>i,j</sup>, Matthieu Réfrégiers<sup>d</sup>, Goran Rašić<sup>k,l</sup>, Branislav Vlahović<sup>k,l,\*</sup>, Vladimir Djoković<sup>a,\*\*</sup>

<sup>a</sup>*Vinča Institute of Nuclear Sciences, University of Belgrade, P.O. Box 522, 11001 Belgrade, Serbia*

<sup>b</sup>*Department of Chemistry and Biochemistry, University of Notre Dame, 251 Nieuwland Science Hall, Notre Dame, Indiana 46556, USA*

<sup>c</sup>*Faculty of Physics, University of Belgrade, P. O. Box 368, 11001 Belgrade, Serbia*

<sup>d</sup>*DISCO beamline, Synchrotron SOLEIL, F-91192 Gif sur Yvette, France*

<sup>e</sup>*DESIRS beamline, Synchrotron SOLEIL, F-91192 Gif sur Yvette, France*

<sup>f</sup>*Faculty of Mechanical Engineering, University of Belgrade, 11000 Belgrade, Serbia*

<sup>g</sup>*Faculty of Agriculture, University of Belgrade, 11000 Belgrade, Serbia*

<sup>h</sup>*Institute of Technical Sciences, Serbian Academy of Sciences and Arts, Belgrade, Serbia*

<sup>i</sup>*Inserm Unité 1193, F-94800 Villejuif, France*

<sup>j</sup>*Univ. Paris-Sud XI, UMR-S1193, F-94800 Villejuif, France*

<sup>k</sup>*North Carolina Central University, Durham, NC 27707, USA*

<sup>l</sup>*NASA University Research Center for Aerospace Device Research and Education and NSF Center of Research Excellence in Science and Technology Computational Center for Fundamental and Applied Science and Education, NC, USA*

---

\* Corresponding author: [vlahovic@nccu.edu](mailto:vlahovic@nccu.edu)

\*\* Corresponding author: [djokovic@vin.bg.ac.rs](mailto:djokovic@vin.bg.ac.rs)

## ABSTRACT

The interaction of partially reduced graphene oxide (prGO) and Huh7.5.1 liver cancer cells was investigated by means of DUV fluorescence bioimaging. The prGO sample was obtained by the reduction (to a certain extent) of the initially prepared graphene oxide (GO) nanosheets with hydrazine. The fluorescence of the GO nanosheets increases with time of the reduction due to a change in ratio of the  $sp^2$  and  $sp^3$  carbon sites and the prGO sample was extracted from the dispersion after 6 min, when the intensity of the fluorescence reached its maximum. The reduction process was left to proceed further to saturation until highly reduced graphene oxide (denoted here as rGO) was obtained. GO, prGO and rGO samples were investigated by structural (scanning electron microscopy (SEM), scanning transmission electron microscopy coupled with energy dispersive spectrometry (STEM-EDS)) and spectroscopic (UV-vis, photoluminescence (PL), Raman) methods. After that, Huh7.5.1 cells were incubated with GO, prGO and rGO nanosheets and used in bioimaging studies, which were performed on DISCO beamline of synchrotron SOLEIL. It was found that the prGO significantly enhanced the fluorescence of the cells and increased the intensity of the signal by ~2.5 times. Time-lapse fluorescence microscopy experiments showed that fluorescence dynamics strongly depends on the type of nanosheets used. The obtained prGO nanostructure can be easily conjugated with aromatic ring containing drugs, which opens a possibility for its applications in fluorescence microscopy monitored drug delivery.

Keywords: bioimaging, graphene oxide, fluorescence, cancer, cells

## 1. Introduction

Graphene-based nanomaterials recently emerged as novel carriers in drug delivery applications [1,2]. Graphene oxide (GO) and reduced GO (rGO) display advantageous characteristics as biosensing platforms due to the high surface area, excellent biocompatibility and ability to interact with proteins and polysaccharides [3-5]. GO exhibits wide fluorescence emission (280 - 500 nm) [6] that can be used to track the transport of the graphene-based nanocarriers to the particular cells by means of fluorescent microscopy [7]. In fluorescent bioimaging, it is also important to use hydrophilic probes with well-defined sizes and specific optical properties. It was shown that the optical properties of GO could be controlled by changing its surface chemistry [8-10]. GO is an electronically hybrid material that possesses both conducting  $\pi$ -states from  $sp^2$  carbon sites and a large energy gap between the  $\sigma$ -states of its  $sp^3$ -bonded carbons. The control of the ratio of the  $sp^2$  and  $sp^3$  fractions by the reduction process enables one to tune its bandgap and, therefore, to controllably transform GO from an insulator to a graphene-like semi-conductor [11]. With the partial reduction of GO, it is possible to influence the size of  $sp^2$  clusters, which affects the fluorescence emission and enhances the quantum yield [8]. In the present study, we decided to investigate the interaction of this intermediate form, partially reduced graphene oxide (prGO), with cancer liver cells (Huh7.5.1 cell line) by using DUV fluorescence microscopy. We believe that the pronounced fluorescence of prGO will enable its easier detection in the certain cell compartments, which is very important if these nanostructures are going to be used in drug delivery applications.

The interaction of graphene-based nanosheets with live cells may induce significant changes in the functioning of the cells and distinct toxic effects. Previous optical microscopy

1  
2  
3 studies revealed that GO and rGO are internalized in cells in a different way, while their toxicity  
4 is highly dependent on the presence of the surface oxygen groups [12,13]. The changes in the  
5 metabolism may be followed by observing the changes in the autofluorescence of the cells, since  
6 autofluorescent species, particularly aromatic amino acids and NADH, are involved in  
7 mitochondrial function, energy metabolism, calcium homeostasis, gene expression, oxidative  
8 stress, aging and apoptosis [14,15]. The study is focused on the fluorescence properties of the  
9 cancer Huh7.5.1 cells after their interaction with GO, prGO and rGO sheets. We also followed  
10 the changes in fluorescence dynamics of these graphene oxide-based species when they are in  
11 contact with the cells.  
12  
13  
14  
15  
16  
17  
18  
19  
20  
21  
22  
23  
24  
25

## 26 **2. Materials and methods**

### 27 *2.1 Graphene oxide and the reduced graphene oxide*

28  
29  
30  
31  
32  
33 Graphene oxide was synthesized by using modified Hummers method according to the  
34 procedure found in ref. [16]. A 150 g of expanded graphite (EG) was used as a starting material,  
35 while sulphuric acid (95-98% H<sub>2</sub>SO<sub>4</sub>, Sigma Aldrich) was used as the intercalating compound.  
36 Sulphuric acid (6 ml) was added to the pillled pieces of EG and mixed at 0 °C for two hours. The  
37 mixture was left overnight and kept at room temperature. Oxidation was carried out by adding  
38 450 mg of potassium permanganate (KMnO<sub>4</sub>). After adding 28 ml of DI water, the mixture was  
39 kept in oil bath at 90-95 °C for two hours. Then, the oxidized graphite mixture was cooled down  
40 to the room temperature. A possible reduction of the product was stopped by adding 84 ml of 3%  
41 solution of H<sub>2</sub>O<sub>2</sub>. Several cycles of centrifugation (at 5500 rpm) and washing with 5% HCl  
42 solution were conducted until brown solution of graphite oxide (GtO) was obtained. The  
43  
44  
45  
46  
47  
48  
49  
50  
51  
52  
53  
54  
55  
56  
57  
58  
59  
60

1  
2  
3 sonication of GO solution with Branson W-450 D Digital Sonifier with 20% amplitude (80W)  
4 for 10 minutes resulted in a change of colour from light brown to light yellow. Transparent light  
5 yellow supernatants of GO were obtained after another cycle of centrifugation and washing.  
6  
7

8  
9  
10 The reduction of the obtained GO was carried out by using 30% solution of hydrazine  
11 hydrate ( $N_2H_4$ , Sigma Aldrich). First, the beaker with 0.1 mg/ml of GO solution was heated in oil  
12 bath at 95°C. After that, 100  $\mu$ l of hydrazine solution was added into heated GO solution to  
13 initiate the reduction process. At certain time intervals during the reduction, equal amounts of  
14 graphene oxide were extracted and diluted with DI water in order to stop the process. The  
15 partially reduced GO samples extracted at different reduction times were stable for more than a  
16 month after the preparation. The reduced GO sample was obtained at the end of the preparation  
17 procedure (after 45 min of reduction). It was less stable; the sheets tended to agglomerate after  
18 few days. This sample was studied immediately after its preparation.  
19  
20  
21  
22  
23  
24  
25  
26  
27  
28  
29

## 30 31 *2.2 Methods*

32  
33 The morphology of graphene oxide was investigated by using a JEOL JSM-6390 scanning  
34 electron microscope (SEM). Because of the low electrical conductivity of graphene oxide, the  
35 surface was covered with thin layer of gold. The micrographs of GO were obtained with ~~x4300~~  
36 magnification and at operating voltage value of 13 kV.  
37  
38  
39  
40  
41

42 The structure and morphology of the GO, prGO and rGO samples were investigated by probe  
43 aberration corrected scanning transmission electron microscope (STEM) (FEI Titan 80-300)  
44 coupled with a SuperX energy dispersive spectrometer (SuperX EDS) with the four silicon drift  
45 detectors (SDD) (Bruker). Aqueous dispersions of the GO, prGO and rGO were deposited on  
46 carbon coated copper grids using an automatic pipette. The samples were left to dry under  
47 ambient conditions before they were transferred to the microscope chamber.  
48  
49  
50  
51  
52  
53  
54  
55  
56  
57  
58  
59  
60

1  
2  
3 A fully automated Raman microscope (LabRAM HR Evolution) was used for Raman  
4 spectroscopy measurements. The spectra were obtained over the Raman shift range from 1000 to  
5 2000  $\text{cm}^{-1}$  using acquisition time of 10 s. The samples were excited by 532 nm laser light (with  
6 1.08 mW of incident power) and the data were collected by using a 50 $\times$  objective.  
7  
8  
9

10  
11  
12 The UV–vis absorption measurements of the aqueous dispersions were carried out on a  
13 Thermo Evolution 600 spectrophotometer.  
14  
15

16  
17 The photoluminescence spectra of aqueous dispersions of GO, prGO and rGO were recorded  
18 using a PerkinElmer LS45 fluorescence spectrophotometer. Fluorescence excitation emission  
19 matrices were recorded on a Fluorolog-3 spectrofluorometer system (Model FL3-221, Horiba  
20 Jobin Yvon). Xenon lamp (450 W) was used as an excitation source. Both excitation and  
21 emission monochromators were double grating, with dispersion of 2.1 nm/mm (1200  
22 grooves/nm). All measurements were performed in the front face geometry at room temperature.  
23 To obtain the fluorescence excitation emission matrices, the emission spectra were recorded in  
24 the range from 330 to 650 nm at 2 nm steps and in the excitations range from 270 to 430 nm at  
25 2.5 nm steps. For these measurements, excitation slit was set at 6 nm, emission slit was at 2 nm  
26 and integration time was fixed to 0.4 ms. Variations of the excitation power were corrected using  
27 reference photodetector.  
28  
29  
30  
31  
32  
33  
34  
35  
36  
37  
38  
39  
40  
41

### 42 *2.3 Cell line and the preparation of biological samples*

43

44 Human hepatocellular carcinoma-derived Huh7.5.1 cells were routinely cultured as  
45 monolayer and were grown in Dulbecco's modified Eagle's medium (DMEM) supplemented  
46 with 10% fetal calf serum, penicillin and streptomycin. The cells were maintained at 37 °C in a  
47 humidified atmosphere of 5%  $\text{CO}_2$ .  
48  
49  
50  
51  
52  
53  
54  
55  
56  
57  
58  
59  
60

1  
2  
3 For DUV fluorescence imaging studies, the Huh7.5.1 cells were plated in plastic Petri dishes  
4 containing 25 mm round quartz coverslip and incubated for 24 hours. Cell attachment was  
5 monitored by visible inspection using a microscope. Thereafter, cells were incubated with GO,  
6 prGO and rGO sheets for 5 hours. The cell's culture medium (3 ml) was mixed with 300  $\mu$ l of  
7 the GO, prGO and rGO dispersions (30  $\mu$ g/ml). After the incubation, the cells were washed with  
8 PBS, fixed with 4% of PFA, rinsed in distilled water and air dried before being used for  
9 bioimaging. The control sample was prepared in the same way but without adding GO, prGO or  
10 rGO.  
11  
12  
13  
14  
15  
16  
17  
18  
19  
20

#### 21 22 *2.4 Deep-UV fluorescence microscopy*

23  
24 The fluorescence images of Huh7.5.1 cells and Huh7.5.1 cells incubated with GO, prGO and  
25 rGO were acquired on TELEMOS endstation of DISCO beamline (SOLEIL synchrotron facility,  
26 France). Synchrotron light source was monochromatized to provide an excitation wavelength of  
27 270 nm and the flux of the beam was less than  $7 \cdot 10^{10}$  photons/s. DISCO beamline is optimized  
28 for the investigations of the biological samples and the intensity of the beam was adjusted to  
29 minimize the possibility of damaging the cells. The fluorescence of the control and incubated  
30 cells was collected in the [327 - 353 nm], [370 - 410 nm] and [420 - 480 nm] wavelength ranges  
31 for 30 seconds. To ensure consistency of the observations at least 30 different locations (80 x 80  
32  $\mu$ m) were investigated. An ultrafluar 100x glycerin immersion objective (Zeiss, Germany) and  
33 PIXIS 1024-BUV EM-CCD camera (Princeton, USA) were used for recording images. Time-  
34 lapse experiments were performed to study the fluorescence dynamics of the control and  
35 incubated cells. The evolution of the fluorescence signal was followed by recording the  
36 fluorescent image every 2 min for 30 s. FIJI software [17] was employed in order to analyse the  
37  
38  
39  
40  
41  
42  
43  
44  
45  
46  
47  
48  
49  
50  
51  
52  
53  
54  
55  
56  
57  
58  
59  
60



obtained fluorescence images. The normalization of original intensities  $I$  was performed by using following formula:

$$f(t_i) = \frac{I(t_i) - I_{min}}{I_{max} - I_{min}}, \quad (1)$$

where  $f(t_i)$  are the normalized intensities with respect to the minimum ( $I_{min}$ ) and maximum ( $I_{max}$ ) values of the  $\{I(t_i)\}$  set.

### 3. Results and discussion

#### 3.1 Structure and optical properties of GO, prGO and rGO

Modified Hummers method was used for the fabrication of graphene oxide and Figure 1 shows the SEM micrograph of the obtained GO sample. The SEM image of a selected exfoliated thin sheet of GO is shown in Figure 1b.

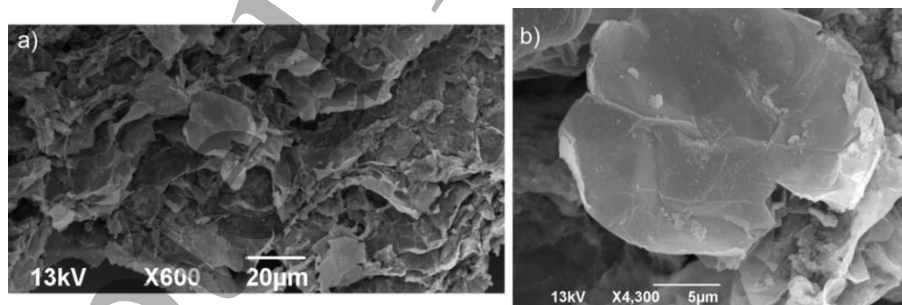
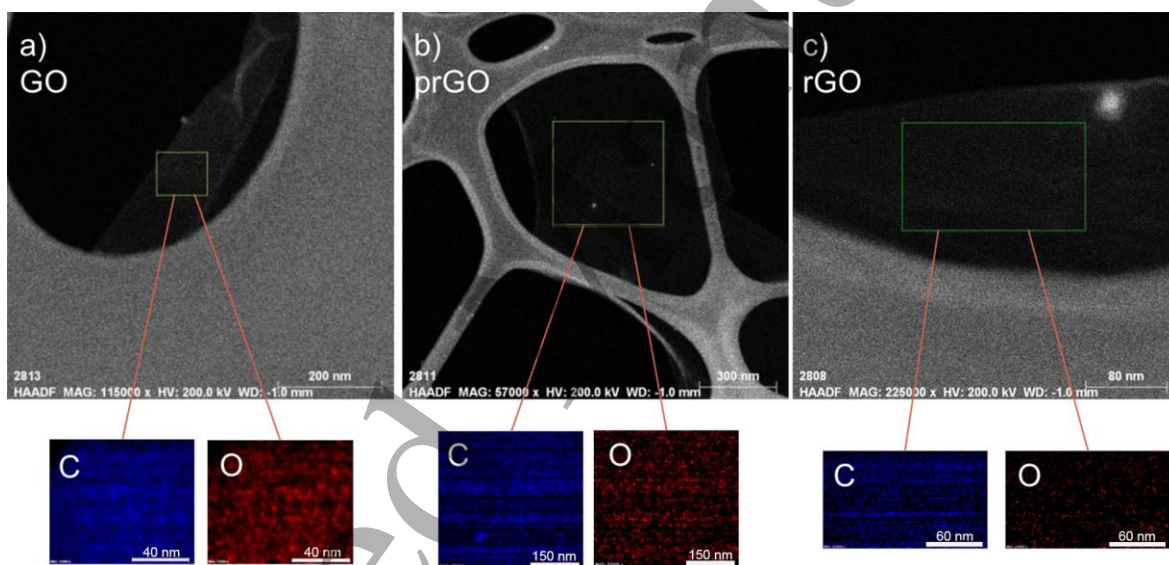


**Fig. 1.** a) Scanning electron microscopy (SEM) micrograph of the obtained GO sheets. B) Selected GO sheet at higher magnification.

As stated in the introduction, the partial reduction of graphene oxide can be used to modify the optical properties of the sheets. It was shown that the reduction process is highly sensitive to the amount of reducing agent (hydrazine) [18-20]. A careful tuning of the concentration of hydrazine

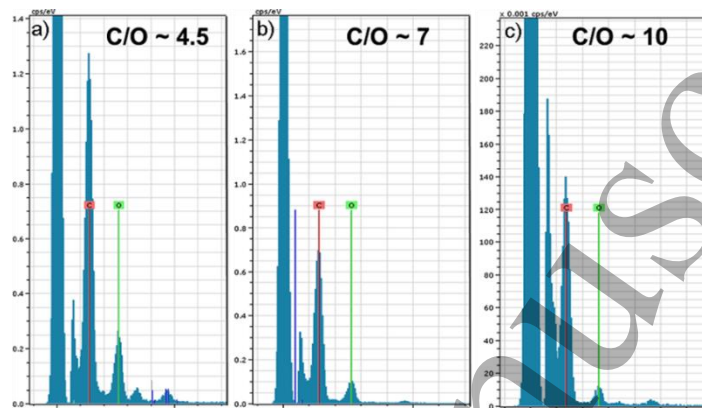
1  
2  
3 and the reduction conditions enabled the extraction of the intermediates with particular  
4 properties. The fluorescence measurements of the intermediate products of the reduction  
5 (Supporting information Figure S1) showed that the GO sample partially reduced for 6 min  
6 exhibited the highest fluorescence intensity. For this reason, the structural and optical  
7 measurements were focused on this particular sample (it will be referred in the text as prGO  
8 unless designated otherwise). Figure 2 shows high-resolution TEM micrographs of the initial  
9 GO, prGO and rGO samples.  
10  
11  
12  
13  
14  
15  
16  
17  
18  
19  
20  
21



22  
23  
24  
25  
26  
27  
28  
29  
30  
31  
32  
33  
34  
35  
36  
37  
38  
39  
40 **Fig. 2.** HRTEM micrographs and elemental maps of carbon and oxygen for a) graphene oxide (GO), b) graphene  
41 oxide partially reduced for 6 min (prGO) and c) reduced graphene oxide (rGO). The elemental composition is  
42 determined for the selected areas on the sheets surfaces (green outlines).  
43  
44  
45  
46  
47

48 The elemental mappings of the highlighted surface areas are shown under the corresponding  
49 TEM images. The oxygen maps (red) reveal that the oxygen content decreases with the time of  
50 reduction (Figure 2). Thus the C/O ratio is increasing with reduction time, which is also  
51 confirmed by EDS results (Figure 3). Fabrication of graphene oxide led to stable 2d  
52  
53  
54  
55  
56  
57  
58  
59  
60

1  
2  
3 nanostructures with  $C/O \sim 4$ . After the reduction,  $C/O$  ratio increased to  $\sim 7$  for prGO and  $\sim 10$  for  
4  
5 rGO. Finally, it is important to mention that the TEM studies reveal that the partial reduction  
6  
7 with hydrazine did not induce visible damage of the layered structures of GO-based species.  
8



9  
10  
11  
12  
13  
14  
15  
16  
17  
18  
19  
20  
21  
22  
23  
24 **Fig. 3.** Energy dispersive spectroscopy (EDS) spectra of a) GO b) prGO and c) rGO samples. The ratios of carbon  
25 and oxygen atoms increase with increasing in reduction time.  
26  
27  
28  
29

30 The changes in carbon-oxygen ratios were also followed by Raman spectroscopy. Figure 4  
31 shows Raman spectra of the GO, prGO and rGO samples with typical D and G peaks at  
32  $1345 \text{ cm}^{-1}$  and  $1588 \text{ cm}^{-1}$  shifts, respectively. The G band originates from the in-plane vibrations  
33 of  $\text{sp}^2$  carbon atoms and represents doubly degenerate phonon mode ( $E_{2g}$  symmetry) at the center  
34 of the Brillouin zone. On the other hand, the D peak ( $A_{1g}$  symmetry mode) comes from the  
35 presence of the  $\text{sp}^3$  carbons and from the defect-induced breathing mode of  $\text{sp}^2$  rings [21,22].  
36 Consequently, the reduction process can be followed by observing the changes in the relative  
37 intensity of these two bands ( $I_D/I_G$ ). The  $I_D/I_G$  ratio of GO is 0.96 and increases after the  
38 reduction to 1.12 and 1.60 for prGO and rGO, respectively (Figure 4). The reduction affects the  
39 in-plane vibrations of  $\text{sp}^2$  carbon atoms, which is reflected in changes in the intensity of the G  
40 mode (Figure 4) [23,24]. Stankovich et al [25] attributed an increase in  $I_D/I_G$  ratio to a decrease  
41 in the average size of the  $\text{sp}^2$  domains upon reduction i.e. to the formation of new graphitic  
42  
43  
44  
45  
46  
47  
48  
49  
50  
51  
52  
53  
54  
55  
56  
57  
58  
59  
60

domains that are smaller in size (~2 nm) than those initially present in GO but, at the same time, more numerous in number. The results presented in Figure 4 are also in agreement with the Raman spectra reported in the other rGO studies where hydrazine hydrate was used as a reduction agent [26,27].

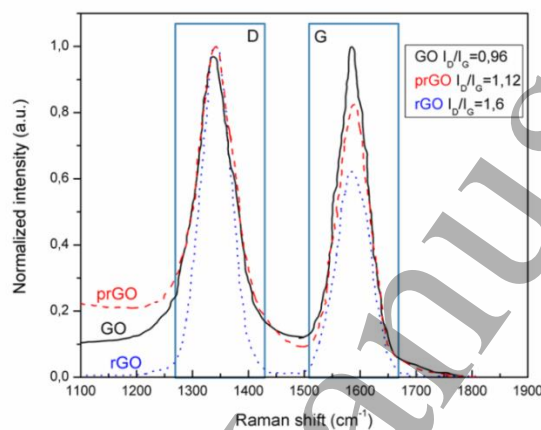


**Fig. 4.** Raman spectra of GO, prGO (GO partially reduced for 6 min) and rGO normalized according to Eq. 1. The rectangles indicate D and G bands and the ratios of their original intensities are given in the inset.

The attenuation of light by GO aqueous dispersions during the reduction process was monitored by UV visible spectroscopy (Figure 5). The absorption spectra of GO dispersion exhibits two peaks at 220 nm and 310 nm which belong to specified transitions of  $\pi-\pi^*$  (C=C) and  $n-\pi^*$  (C=O), respectively. There is a red shift of the absorbance peak at 220 nm during the reduction. It can also be seen that the shoulder at 310 nm disappeared after the reduction, which is attributed to the decrease in concentration of carboxyl groups [8]. The color of the dispersions also changes during the reduction. The photo of the dispersions is given in the inset of Figure 5.

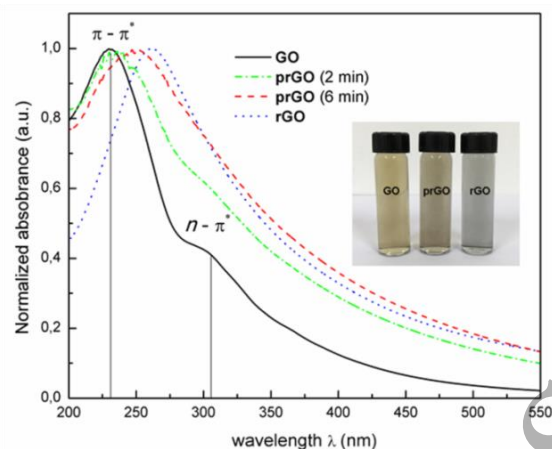


**Fig. 5.** Normalized UV-vis spectra of GO, prGO (partially reduced for 2 and 6 min) and rGO. The inset shows the photo of the obtained GO, prGO (partially reduced for 6 min) and rGO dispersions.

Due to the functionalization (oxidation)-induced opening of the energy gap, GO is expected to exhibit photoluminescence. For the excitation in the UV part of the EM spectrum, GO shows pronounced fluorescence emission between 400 and 500 nm, which originates from radiative recombination of electron-hole pairs located in small  $sp^2$  domains [8]. The intensity of the PL emission strongly depends on the time of reduction of GO. It increases with reduction time, reaches the maximum after 6 min and then starts to decrease. The fluorescence intensity does not change significantly after prolonged reduction ( $> 10$  min). As mentioned above, we will focus on the emission properties of the sample obtained after 6 min of reduction (prGO). PL spectra of the initial GO sample and GO samples reduced at different times are included in Supporting information (Figure S1).

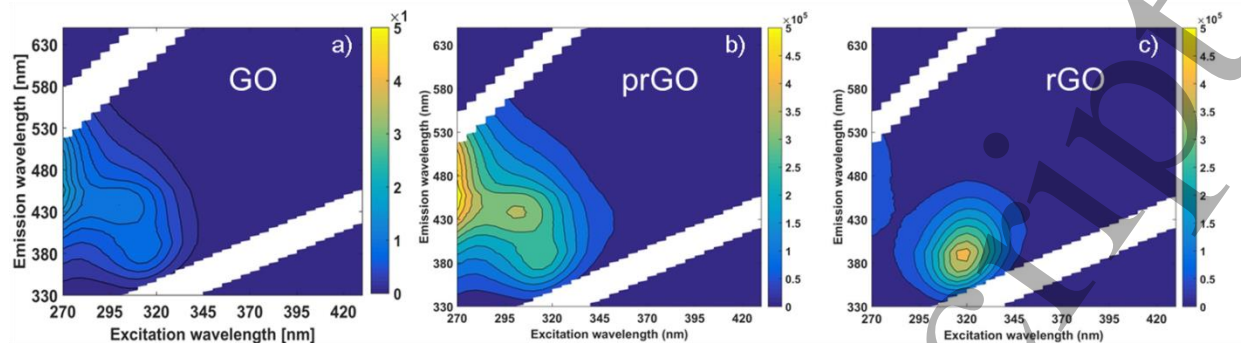


**Fig. 6.** Emission excitation matrices obtained for a) GO, b) prGO and c) rGO samples. The 270 – 430 nm excitation and 330 – 650 nm emission wavelength ranges were used.

The emission excitation matrices of the GO, prGO and rGO are shown in Figure 6. As can be seen, there are two distinct regions with pronounced photoluminescence intensity noted as region I ( $\lambda_{\text{exc}} = 270$  nm,  $\Delta\lambda_{\text{em}} = 380 - 550$  nm) and region II ( $\lambda_{\text{exc}} = 300$  nm,  $\Delta\lambda_{\text{em}} = 350 - 450$  nm). Since we intended to study the interaction of GO-based nanosheets with cancer liver cells by DUV imaging, we were interested in the first region with excitation at 270 nm.

Single emission spectra extracted from the emission excitation matrices for  $\lambda_{\text{exc}} = 270$  nm are shown in Figure 7a.

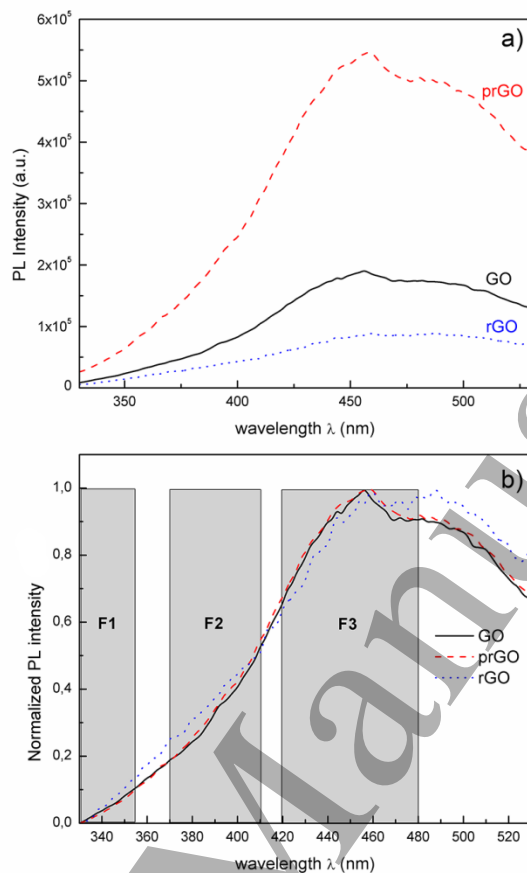


**Fig. 7.** a) Photoluminescence (PL) emission spectra of GO, prGO and rGO obtained at  $\lambda_{\text{exc}} = 270$  nm. b) The same PL spectra normalized with respect to the maximum of the emission intensity. The rectangles indicate the emission ranges F1 [327 – 353 nm], F2 [370 – 410 nm] and F3 [420 – 480 nm] used in deep UV fluorescence imaging

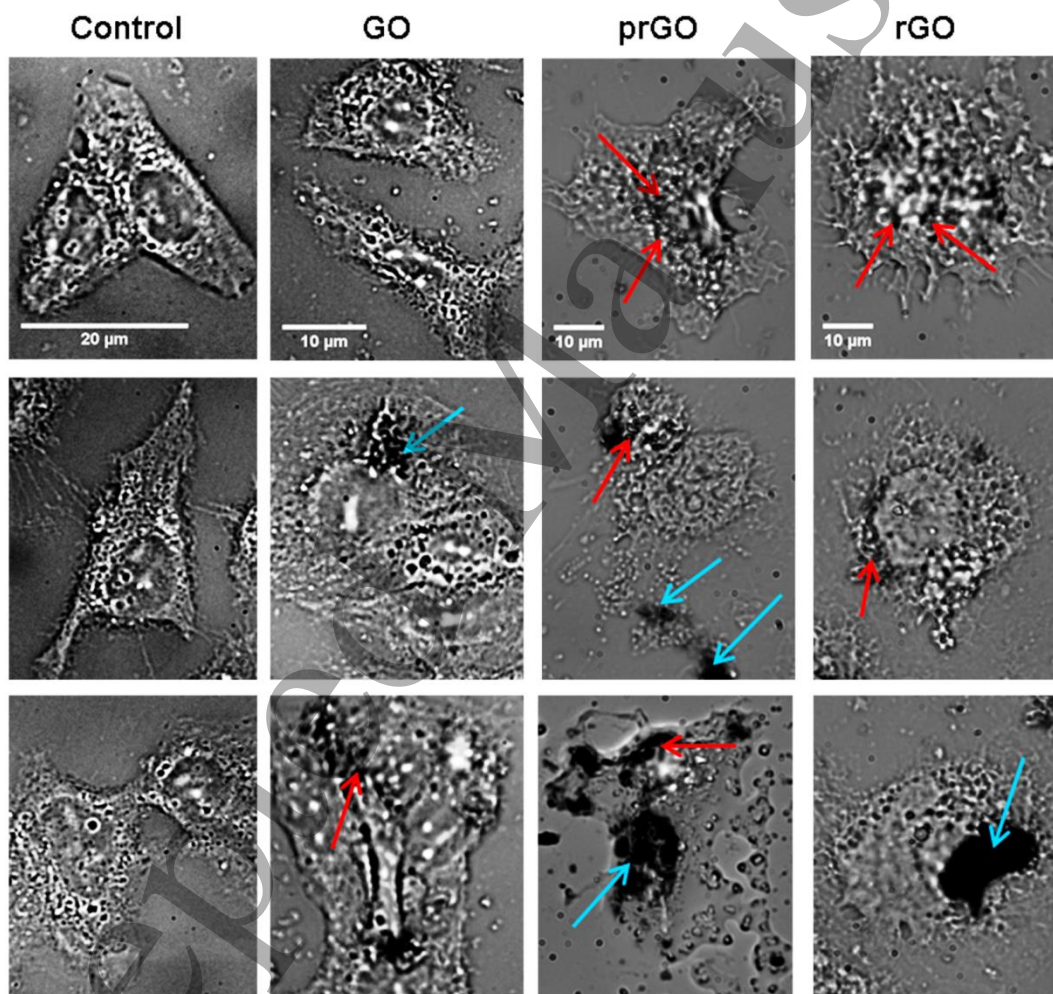
It can be seen that the partially reduced graphene oxide yields the highest fluorescence. Apparently, the partial reduction induced specific rearrangement of the honeycomb network which resulted in more effective recombination of excited electrons that further led to the increase in fluorescence intensity. In Figure 7b, we present the normalized photoluminescence spectra from Figure 7a. The grey rectangles indicate the emission ranges that are used for the collection of the fluorescence signal in DUV imaging: F1 [327 – 353 nm], F2 [370 – 410 nm]



1  
2  
3 and F3 [420 – 480 nm]. Obviously, the maximum of emission is in F3 range, while all three GO-  
4  
5 based species show negligible emission in F1 range.  
6

### 7 3.2 DUV Fluorescence imaging of Huh7.5.1 cells incubated with GO, prGO and rGO

8  
9  
10 Selected visible microscopy images of the control Huh7.5.1 cells and the cells incubated  
11  
12 with GO, prGO and rGO are shown in Figure 8.  
13  
14  
15  
16



49  
50  
51  
52  
53  
54  
55  
56  
57  
58  
59  
60

**Fig. 8.** Bright field micrographs of control Huh 7.1.5 cells (1<sup>st</sup> column) and Huh 7.1.5 cells incubated with GO, prGO and rGO (2<sup>nd</sup>, 3<sup>rd</sup> and 4<sup>th</sup> columns, respectively). Red arrows indicate localization of GO, prGO and rGO at cell sites. Blue arrows indicate non-internalized entities.



1  
2  
3 A careful analysis of the cells from various locations along the samples suggested that the  
4 morphology of the cells was slightly affected by the presence of GO. GO incubated cancer cells  
5  
6 closely resemble the form of the control cells and folded GO aggregates rarely penetrate into the  
7  
8 interior of the cells (Figure 8, the 1<sup>st</sup> and 2<sup>nd</sup> columns). In the case of the cells incubated with  
9  
10 prGO and rGO, they are more affected by the presence of the nanosheets and there are numerous  
11  
12 sites where the sheets are internalized in the cells. It is obvious that degree of the internalization  
13  
14 strongly depends on the presence of surface ligands and, consequently, on the reduction level.  
15  
16 The agglomerates of internalized reduced graphene oxides are indicated by red arrows (Figure 8  
17  
18 the 3<sup>rd</sup> and 4<sup>th</sup> columns). This is in agreement with literature data, which showed that cells had  
19  
20 the ability to internalize, actively fold and compartmentalize relatively large pieces of the sheets  
21  
22 and remain viable [12,13,28-30].  
23  
24  
25  
26  
27

28  
29 Deep UV imaging of treated and untreated Huh7.5.1 cancer liver cells was performed by  
30  
31 using the excitation wavelength of 270 nm and the fluorescence emission was monitored in three  
32  
33 spectral windows F1 [327 – 353 nm], F2 [370 – 410 nm] and F3 [420 – 480 nm]. GO, prGO and  
34  
35 rGO fluorescence centers have a wide blue emission that primarily falls into the F3 range (Figure  
36  
37 7b), and partially into the F2 range. The Huh7.5.1 cells have intrinsic fluorescence that has been  
38  
39 detected in all three spectral emission ranges, with comparable fluorescence intensities. Bright  
40  
41 field and corresponding fluorescent images of the control and incubated cells in F3 emission  
42  
43 range are shown in Figure 9. In the second row of Figure 9, we show LUT fluorescent images of  
44  
45 the cells, while in the fourth row are the same images normalized with respect to the highest  
46  
47 intensity observed for the prGO incubated sample for comparison purposes. As can be seen, the  
48  
49 fluorescence of GO-incubated is similar to the fluorescence of the control cells (Figure 9, the 2<sup>nd</sup>  
50  
51 and 4<sup>th</sup> row). Also, the fluorescence emission in both samples is mainly homogeneously  
52  
53  
54  
55  
56  
57  
58  
59  
60

distributed in the cytoplasmic region. On the other hand, the fluorescence intensities of the prGO/Huh and rGO/Huh samples are much higher than the autofluorescence of the control sample.

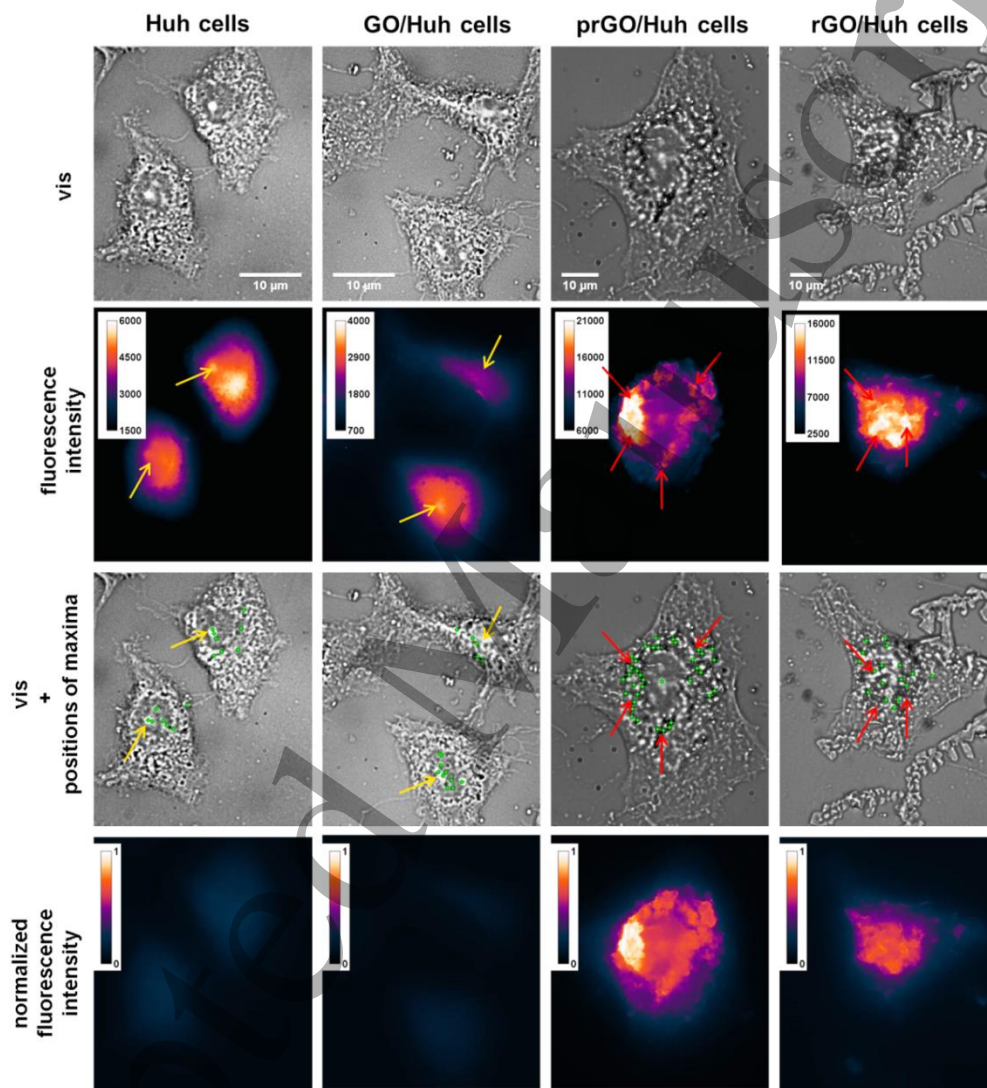


**Fig. 9.** Bright field microscopy (the 1<sup>st</sup> row) and corresponding DUV fluorescent images (the 2<sup>nd</sup> row) of the control and GO, prGO and rGO incubated Huh7.5.1 cells in F3 [420-480 nm] emission range. In the 3<sup>rd</sup> row, the green dots indicate the positions of the local fluorescence maxima (the positions where the intensity of the fluorescence signal exceeds 85% of the maximum fluorescence intensity). The 4<sup>th</sup> row shows fluorescence images of control and GO, prGO and rGO incubated cells normalized with respect to the maximum intensity obtained for prGO incubated cells.

1  
2  
3 Furthermore, it seems that the maxima of the fluorescence coincide with the cell compartments  
4 containing internalized prGO and rGO species. In order to show this more clearly, we introduced  
5 bright field images with marked positions of the fluorescence maxima (green dots) in the third  
6 row of Figure 9. To establish the positions of the maxima, the signal intensities were scaled to  
7 include the fluorescence that exceeds >85% of the maximum intensity (the details about the  
8 scaling procedure and maxima selections can be found in Supporting information, Figure S2). It  
9 is well known that the nucleoli are the brightest intracellular autofluorescent sites [14,31] in the  
10 nuclei and this is indeed true for the control and GO+Huh samples (the nucleoli are indicated by  
11 yellow arrows). In the case of prGO+Huh and rGO+Huh samples, the maxima are positioned on  
12 the black entities (indicated by red arrows) suggesting that the fluorescence comes from  
13 internalized prGO and rGO. We have selected typical DUV fluorescent images of the control as  
14 well as GO, prGO and rGO incubated cells, but the similar fluorescent behavior was noticed at  
15 different locations along the sample (the additional images were included in Supporting  
16 information, Figure S3). It is important to notice that the prGO and rGO aggregates localized in  
17 the vicinity of the cells do not fluoresce. The lower fluorescence intensity of the prGO (or rGO)  
18 aggregates located outside the cell is a consequence of the agglomeration of the sheets. The  
19 agglomeration results in the formation of  $\pi$ -stacked complexes, which in turn induces a static  
20 quenching [32]. This effect is less pronounced in the case of internalized prGO/rGO because the  
21 intracellular material may separate the sheets and prevent the  $\pi$ - $\pi$  stacking. Further, we calculated  
22 the average fluorescent intensities per single cell (number of cells  $n > 30$ ) for all 4 samples,  
23 which are presented in Figure 10. The results show that the cells with internalized prGO  
24 nanostructures have 2.5 times higher fluorescence intensity in F3 range than that of the control  
25 samples. It can also be seen that the average fluorescence intensities in all three spectral ranges  
26  
27  
28  
29  
30  
31  
32  
33  
34  
35  
36  
37  
38  
39  
40  
41  
42  
43  
44  
45  
46  
47  
48  
49  
50  
51  
52  
53  
54  
55  
56  
57  
58  
59  
60

1  
2  
3 decrease slightly after incubation with GO. It is possible that GO quenches the main cell  
4 fluorophores such as tryptophan, tyrosine, phenylalanine and NADH [33,34]. Nevertheless, the  
5  
6  
7  
8 observed changes are within the experimental error (Figure 10). An increase in the fluorescence  
9  
10  
11  
12  
13  
14  
15  
16  
17  
18  
19  
20  
21  
22  
23  
24  
25  
26  
27  
28  
29  
30  
31  
32  
33  
34  
35  
36  
37  
38  
39  
40  
41  
42  
43  
44  
45  
46  
47  
48  
49  
50  
51  
52  
53  
54  
55  
56  
57  
58  
59  
60

decrease slightly after incubation with GO. It is possible that GO quenches the main cell fluorophores such as tryptophan, tyrosine, phenylalanine and NADH [33,34]. Nevertheless, the observed changes are within the experimental error (Figure 10). An increase in the fluorescence intensity of Huh7.5.1 cells incubated with rGO, relative to those treated with GO, could be attributed to better internalization of rGO by the cells and consequently reduced  $\pi$ - $\pi$  stacking. These observations are confirmed by additional DUV fluorescent microscopy measurements on another set of samples. Obviously, the presence of the reduced GO nanostructures affects the overall fluorescence of the Huh7.5.1 cells. We further investigated the fluorescence dynamics with consecutive imaging of the treated and untreated cells.

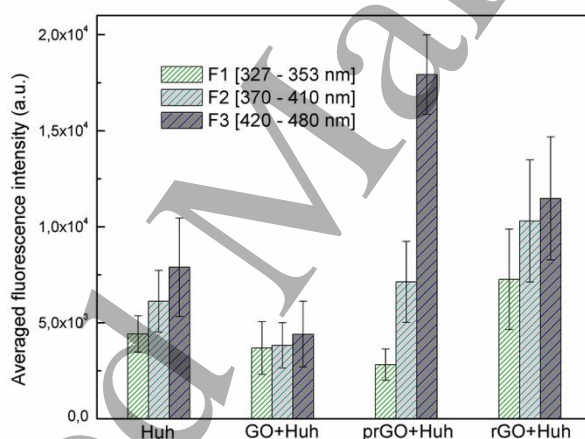


**Fig. 10.** The average fluorescent intensity per single cell for untreated Huh7.5.1 cells (control), as well as GO, prGO and rGO, incubated Huh7.5.1 cells (number of cells counted  $n > 30$ ). The error bars represent standard deviations of the fluorescence intensity.

Selected local fluorescent maxima are followed in the time-lapse experiment (see Figure S4 in Supporting information for details). The time dependence of the average intensity of local maxima (normalized according to Eq. 1) in F1, F2 and F3 emission ranges are shown in

Figure 11. The original average intensities at particular time intervals and the standard deviations are given in Supporting information (Table S1).

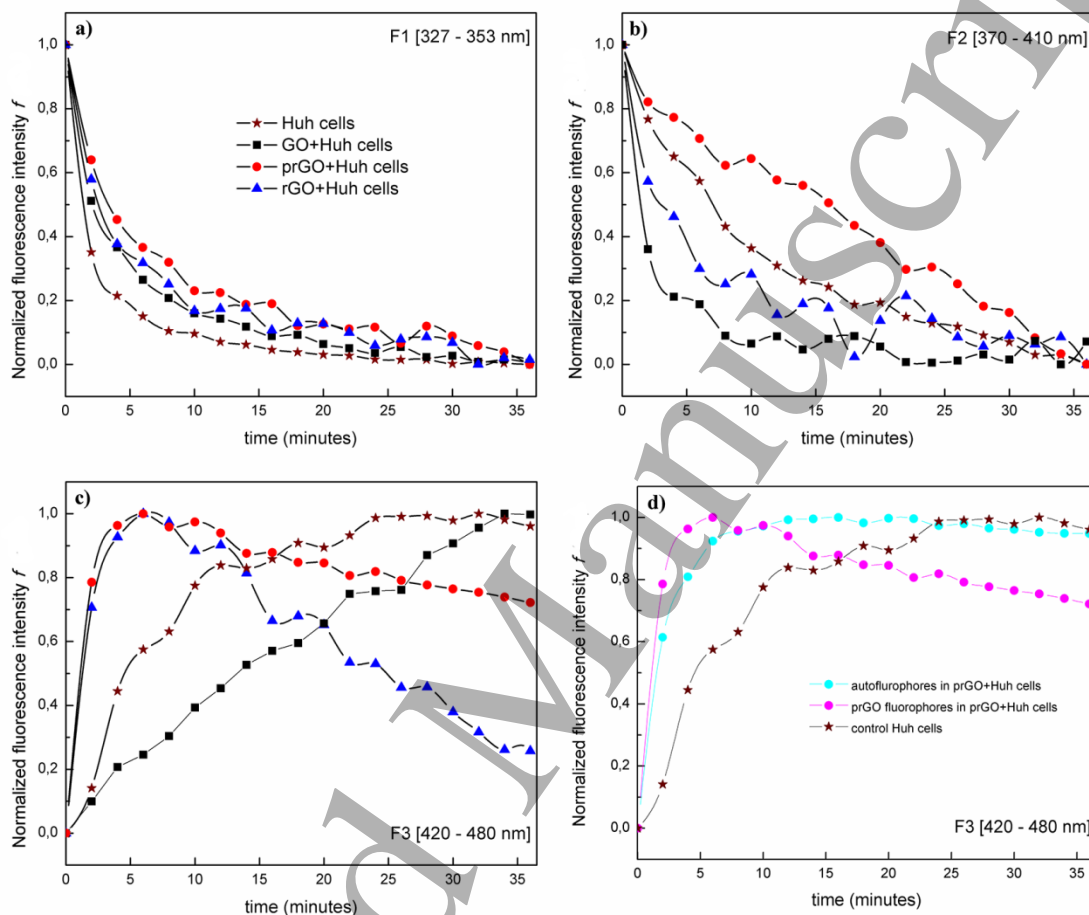


**Fig. 11.** The dependences of the average intensities of local maxima (normalized according to Eq. 1) from time in a) F1 [327-353 nm] b) F2 [370-410 nm] and c) F3 [420-480 nm] emission ranges. D) The evolution of the fluorescent signal that comes from the autofluorophores (fluorescent maxima previously fixed by observing the fluorescence in the F1 range) and from prGO fluorophores in the F3 range (the details about the procedure of finding maxima are explained in the Supporting information, Figure S5). The curve that corresponds to control Huh cells in c) is also included in d) for comparison.

It can be seen that the presence of graphene oxide based species does not influence the fluorescence kinetics significantly in F1 range. The incubated and control cells show similar

1  
2  
3 time-dependence of the fluorescence intensity (Figure 11a). The fluorescent intensity decreases  
4 with prolonged time, with the slowest decay noticed in the case of the prGO+Huh cells. The time  
5 dependence of the fluorescence intensity does not change significantly when the detection was  
6 switched from F1 to F2 window (Figure 11b). The intensity decreases with time in this range as  
7 well. However, the degrees of changes are more pronounced. Also, the fastest intensity decay  
8 was observed for the GO incubated cells and it should be attributed to the GO-induced emission  
9 quenching of tryptophan-containing species mentioned above [33]. In the F3 range (Figure 11c),  
10 the dependence of the fluorescence intensity from time is somewhat different. As can be seen in  
11 Figure 11c, the normalized fluorescence intensity of the control cells increases with time. Their  
12 fluorescence mostly originates from the presence of NADH, which exhibits maximum  
13 fluorescence in this range [15]. Also, the time dependence of the fluorescence intensity of the  
14 pure NADH material [35] is similar to that of the control cells observed in Figure 11c.

15  
16  
17  
18  
19  
20  
21  
22  
23  
24  
25  
26  
27  
28  
29  
30  
31 It should also be noticed that the fluorescence of the cells incubated with graphene oxide  
32 increases almost linearly with time, while the increase itself is slower than that observed for the  
33 untreated cells. On the other hand, the reduced graphene oxides (prGO and rGO) affect the  
34 fluorescence dynamics differently. The time-lapse experiments show that the fluorescence  
35 intensities of prGO and rGO incubated cells reach maxima after approximately 6 minutes and  
36 then start to decrease (Figure 11c). The obtained results apparently show that GO, prGO and  
37 rGO nanosheets affect the fluorescence dynamics in a different way. GO obviously interacts with  
38 the cells' autofluorophores, tryptophan (main fluorescence in the F2 range) and NADH (main  
39 fluorescence in the F3 range), and induces partial quenching through non-radiative processes.  
40  
41  
42  
43  
44  
45  
46  
47  
48  
49  
50  
51  
52  
53  
54  
55  
56  
57  
58  
59  
60  
The time-lapse measurements in the F3 range showed the presence of two general processes in  
the fluorescence of prGO and rGO incubated Huh7.5.1 cells in contrast to the continuous

1  
2  
3 increasing of the fluorescence of the control cells. In Figure 11d, we tried to follow the time  
4 dependence of the fluorescence intensities of the autofluorophore (NADH) and fluorophore  
5 prGO in the prGO incubated cells separately. The details of the procedure are explained in the  
6 Supporting information (Figure S5). Briefly, the positions of the fluorescence maxima in F1  
7 range (which correspond almost exclusively to the fluorescence of the autofluorophores) were  
8 fixed. After that, the time evolution of these fluorescence centers was followed in the F3 range  
9 together with the time evolution of strongest fluorescence centers in the same range (which  
10 coincide with the positions of prGO sheets). As the results in Figure 11d show, the fluorescence  
11 dynamics of the autofluorophores in the F3 range closely resembles the dynamics of control cells  
12 in the same range. The fluorescence intensity is increasing with time until it reaches saturation.  
13 This suggests that the change in fluorescence dynamics of prGO+Huh cells with respect to that  
14 of the control cells is indeed the consequence of the presence of prGO fluorophores. A deeper  
15 understanding of the effects of prGO on the time evolution of fluorescent signal would require a  
16 separate study. Nevertheless, the presented results (Figures 9 and 10) clearly show that the  
17 average fluorescence intensity of the cells significantly increases if they are incubated with prGO  
18 sample. Since it contains both  $sp^2$  and  $sp^3$  domains, it may interact with aromatic ring containing  
19 drugs through  $\pi$ - $\pi$  stacking but also with polar molecules via epoxide, hydroxyl, and carboxylic  
20 groups. This is why we believe that prGO can also be used in drug delivery applications. The  
21 successful delivery of the drug conjugated to prGO nanosheets might be monitored by  
22 fluorescence imaging and we plan to continue our research in this direction.  
23  
24  
25  
26  
27  
28  
29  
30  
31  
32  
33  
34  
35  
36  
37  
38  
39  
40  
41  
42  
43  
44  
45  
46  
47  
48  
49  
50

#### 51 **4. Conclusion**

52  
53  
54  
55  
56  
57  
58  
59  
60

1  
2  
3 In this article, DUV fluorescence spectroscopy was used to study the interaction of partially  
4 reduced graphene oxide with the cancer liver cells. A modified Hummers method was used for  
5 the fabrication of graphene oxide and the reduction was performed in the presence of hydrazine  
6 hydrate. The partial reduction of graphene oxide was achieved by controlling the duration of the  
7 reduction process. It was found that the sample partially reduced for 6 min showed the highest  
8 fluorescence intensity and it was further used in bioimaging tests. GO, prGO and rGO samples  
9 were studied using various microscopy and spectroscopic methods in order to establish their  
10 structure and physical properties. STEM micrographs of GO, prGO and rGO showed the  
11 presence of isolated monolayers. Elemental analysis revealed that the C/O ratio values were  
12 dependent on the time of reduction, which was also confirmed by Raman spectroscopy. The  
13 change in the optical properties was monitored by photoluminescence and UV-vis  
14 spectroscopies. The partially reduced graphene oxide showed the highest intensity of  
15 photoluminescence emission for the excitation that belongs to the DUV part of the EM spectrum.  
16 The fluorescent GO, prGO and rGO nanostructures were used in the DUV fluorescence imaging  
17 study of the cancer liver cell line Huh7.5.1. The interaction of the prGO nanostructures with the  
18 cells resulted in a strong increase in the fluorescence intensity in F3 [420-480 nm] range with  
19 respect to the autofluorescence of the control sample. Time-lapse studies showed that the time  
20 dependence of the fluorescence emission from GO, prGO and rGO internalized cells is different  
21 from that of the intrinsic fluorescence of the untreated cells. The prGO nanostructure was  
22 suggested as a possible carrier for cancer drugs since its pronounced fluorescence might be used  
23 for monitoring the delivery process. In the forthcoming study, we will focus on the drug  
24 conjugated-prGO nanostructures and their interaction with cancer cells.  
25  
26  
27  
28  
29  
30  
31  
32  
33  
34  
35  
36  
37  
38  
39  
40  
41  
42  
43  
44  
45  
46  
47  
48  
49  
50  
51  
52  
53  
54  
55  
56  
57  
58  
59  
60



## Acknowledgements

Deep UV imaging was performed at the DISCO beamline of Synchrotron SOLEIL (France). This study was financially supported by Ministry of Education and Science and Technological Development, Republic of Serbia (Project Nos. 172056, 45020 and 171029) and projects NSF CREST (HRD-0833184) and NASA (NNX09AV07A).

## References

- [1] C. Cheng, S. Li, A. Thomas, N. A. Kotov, R. Haag, Functional graphene nanomaterials based architectures: biointeractions, fabrications, and emerging biological applications, *Chem. Rev.* 117 (2017) 1826-1914.
- [2] D. Du, Y. Yang, Y. Lin, Graphene-based materials for biosensing and bioimaging, *MRS Bull.* 37 (2012) 1290-1296.
- [3] S. Mahanta, S. Paul, Bovine  $\alpha$ -lactalbumin functionalized graphene oxide nano-sheet exhibits enhanced biocompatibility: A rational strategy for graphene-based targeted cancer therapy, *Colloids Surf. B Biointerfaces* 134 (2015) 178-187.
- [4] S. Zhang, K. Yang, L. Feng, Z. Liu, In vitro and in vivo behaviors of dextran functionalized graphene, *Carbon* 49 (2011) 4040-4049.
- [5] C. Lu, P.-J. J. Huang, B. Liu, Y. Ying and J. Liu, Comparison of graphene oxide and reduced graphene oxide for DNA adsorption and sensing, *Langmuir* 32 (2016) 10776-10783.
- [6] C. Lu, P.-J. J. Huang, B. Liu, Y. Ying and J. Liu, Exploring the origin of blue and ultraviolet fluorescence in graphene oxide, *J. Phys. Chem. Lett.* 4 (2013) 2035-2040.

1  
2  
3 [7] A. P. Demchenko, M. O. Dekaliuk Novel fluorescent carbonic nanomaterials for sensing  
4 and imaging. *Methods Appl. Fluoresc.* 1 (2013) 042001 (17pp)

5  
6  
7 [8] G. Eda, Y.-Y. Lin, C. Mattevi, H. Yamaguchi, H.-A. Chen, I.-S. Chen, C.-W. Chen, M.  
8 Chhowalla, Blue photoluminescence from chemically derived graphene oxide, *Adv. Mater.* 22  
9 (2010) 505-509.

10  
11  
12 [9] G. Xin, Y. Meng, Y. Ma, D. Ho, N. Kim, S. M. Cho, H. Chae, Tunable photoluminescence  
13 of graphene oxide from near-ultraviolet to blue, *Mater. Lett.* 74 (2012) 71-73.

14  
15 [10] C.-T. Chien, S.-S. Li, W.-J. Lai, Y.-C. Yeh, H.-A. Chen, I.-S. Chen, L.-C. Chen, K.-H.  
16 Chen, T. Nemoto, S. Isoda, M. Chen, T. Fujita, G. Eda, H. Yamaguchi, M. Chhowalla, C.-W.  
17 Chen, Tunable photoluminescence from graphene oxide, *Angew. Chem. Int. Ed.* 51 (2012) 6662-  
18 6666.

19  
20 [11] N. Morimoto, T. Kubo, Y. Nishima, Tailoring the oxygen content of graphite and reduced  
21 graphene oxide for specific applications, *Sci. Rep.* 6 (2016) 21715 (8pp).

22  
23 [12] N. Chatterjee, H. J. Eom and J. Choi, A systems toxicology approach to the surface  
24 functionality control of graphene-cell interactions, *Biomaterials* 35 (2014) 1109-1127.

25  
26 [13] S. J. Corr, M. Raouf, B. T. Cisneros, O. Kuznetsov, K. Massey, W. D. Kaluarachchi. M.  
27 A. Cheney, E. W. Billups, L. J. Wilson, S. A. Curley, Cytotoxicity and variant cellular  
28 internalization behavior of water-soluble sulfonated nanographene sheets in liver cancer cells,  
29 *Nanoscale Res. Lett.* 8 (2013) 208 (10pp).

30  
31 [14] M. Monici, Cell and tissue autofluorescence research and diagnostic applications,  
32 *Biotechnol. Annu. Rev.* 11 (2005) 227-256.

33  
34 [15] A. A. Heikal, Intracellular coenzymes as natural biomarkers for metabolic activities and  
35 mitochondrial anomalies, *Biomark. Med.* 4 (2010) 241-263.

36  
37  
38  
39  
40  
41  
42  
43  
44  
45  
46  
47  
48  
49  
50  
51  
52  
53  
54  
55  
56  
57  
58  
59  
60

1  
2  
3 [16] C. Galande, A. D. Mohite, A. V. Naumov, W. Gao, L. Ci, A. Ajayan, H. Gao, A.  
4 Srivastava, R. Bruce Weisman & P. M. Ajayan, Quasi-molecular fluorescence from graphene  
5 oxide, *Sci. Rep.* 1 (2011) Art. number: 85  
6  
7

8  
9  
10 [17] J. Schindelin, I. Arganda-Carreras, E. Frise, V. Kaynig, M. Longair, T. Pietzsch, S.  
11 Preibisch, C. Rueden, S. Saalfeld, B. Schmid, J. Y. Tinevez, D. J. White, V. Hartenstein, K.  
12 Eliceiri, P. Tomancak, A. Cardona, Fiji: an open-source platform for biological-image analysis,  
13 *Nat. Methods* 9 (2012) 676.  
14  
15

16  
17 [18] X. Gao, J. Jang, S. Nagase, Hydrazine and thermal reduction of graphene oxide: reaction  
18 mechanisms, product structures, and reaction design, *J. Phys. Chem. C* 114 (2010) 832.  
19  
20

21  
22 [19] C. K. Chua, M. Pumera, The reduction of graphene oxide with hydrazine: elucidating its  
23 reductive capability based on a reaction-model approach, *Chem. Comm.* 52 (2015) 72-75.  
24  
25

26  
27 [20] C. K. Chua, M. Pumera, Chemical reduction of graphene oxide: a synthetic chemistry  
28 viewpoint, *Chem. Soc. Rev.* 43 (2014) 291-312.  
29  
30

31  
32 [21] C. Ferrari, J. Robertson, Interpretation of Raman spectra of disordered and amorphous  
33 carbon, *Phys. Rev. B* 61 (2000) Art No. 14095-14107.  
34  
35

36  
37 [22] F. Tuinstra, J. L. Koenig, Raman spectrum of graphite, *J. Chem. Phys.* 53 (1970)  
38 1126-1130.  
39  
40

41  
42 [23] D. Yang, A. Velamakanni, G. Bozoklu, S. Park, M. Stoller, R. D. Piner, S. Stankovich, I.  
43 Jung, D. A. Field, C. A. Ventrice Jr., R. S. Ruoff, Chemical analysis of graphene oxide films  
44 after heat and chemical treatments by X-ray photoelectron and Micro-Raman spectroscopy,  
45 *Carbon* 47 (2009) 145-152.  
46  
47  
48  
49  
50  
51  
52  
53  
54  
55  
56  
57  
58  
59  
60

1  
2  
3 [24] F. Yin, S. Wu, Y. Wang, L. Wu, P. Yuan, X. Wang, Self-assembly of mildly reduced  
4 graphene oxide monolayer for enhanced Raman scattering, *J. Solid State Chem.* 237 (2016)  
5 57-63.  
6  
7

8  
9  
10 [25] S. Stankovich, D. A. Dikin, R D. Piner, K. A. Kohlhaas, A. Kleinhammes, Y. Jia, Y. Wu,  
11 S. T. Nguyen, R. S. Ruoff, Synthesis of graphene-based nanosheets via chemical reduction of  
12 exfoliated graphite oxide. *Carbon* 45 (2007) 1558–1565.  
13  
14

15  
16  
17 [26] V. C. Tung, M. J. Allen, Y. Yang, R. B. Kaner, High-throughput solution processing of  
18 large-scale graphene, *Nat. Nanotech.* 4 (2009) 25–29.  
19  
20

21  
22 [27] J. I. Paredes, S. Villar-Rodil, P. Solís-Fernandez, A. Martínez-Alonso, J. M. D. Tascon,  
23 Atomic force and scanning tunneling microscopy imaging of graphene nanosheets derived from  
24 graphite oxide, *Langmuir*, 25 (2009) 5957–5968.  
25  
26

27  
28 [28] T. Lammel, P. Boisseaux, M. L. Fernandez-Cruz, J. M. Navas, Internalization and  
29 cytotoxicity of graphene oxide and carboxyl graphene nanoplatelets in the human hepatocellular  
30 carcinoma cell line Hep G2, *Part. Fibre Toxicol.* 10 (2013) 27 (21pp).  
31  
32

33  
34 [29] S. R. Shin, B. Aghaei-Ghareh-Bolagh, X. Gao, M. Nikkhah, S. M. Jung, A. Dolatshahi-  
35 Pirouz, S. B. Kim, S. M. Kim, M. R. Dokmeci, X. S. Tang, A. Khademhosseini, Layer-by-layer  
36 assembly of 3D tissue constructs with functionalized graphene, *Adv. Funct. Mater.* 24 (2014)  
37 6136-6144.  
38  
39

40  
41 [30] J. Park, B. Kim, J. Han, J. Oh, S. Park, S. Ryu, S. Jung, J.-Y. Shin, B. S. Lee, B. H. Hong,  
42 D. Choi, B.-S. Kim, Graphene oxide flakes as a cellular adhesive: prevention of reactive oxygen  
43 species mediated death of implanted cells for cardiac repair, *ACS Nano* 9 (2015) 4987-4999.  
44  
45  
46  
47  
48  
49  
50  
51  
52  
53  
54  
55  
56  
57  
58  
59  
60

1  
2  
3 [31] K. K. Konig, P. T. C. So, W. W. Matulin, B. J. Tromberg, E. Gratton, Two photon excited  
4 lifetime imaging of autofluorescence in cells UVA and NIR photostress, *J. Microsc.* 183 (1996)  
5 197-204.  
6  
7

8  
9  
10 [32] J. Kim, F. Kim, J. Huang, Seeing graphene-based sheets, *Mater. Today* 13 (2010) 28-38.  
11

12 [33] S. Li, A. N. Aphale, I. G. Macwan, P. K. Patra, W. G. Gonzalez, J. Mikovska, R. M.  
13 Leblanc, Graphene oxide as a quencher for fluorescent assay of amino acids, peptides, and  
14 proteins, *ACS Appl. Mater. Interfaces* 4 (2012) 7069-7075.  
15  
16  
17

18  
19 [34] Y. Zhao, H.-S. Hsieh, M. Wang, C. T. Jafvert, Light-independent redox reactions of  
20 graphene oxide in water: Electron transfer from NADH through graphene oxide to molecular  
21 oxygen, producing reactive oxygen species, *Carbon* 123 (2017) 216-222.  
22  
23  
24

25  
26 [35] Y. Zhao, H.-S. Hsieh, M. Wang, C. T. Jafvert, NADH enzyme-dependent fluorescence  
27 recovery after photobleaching (ED-FRAP): applications to enzyme and mitochondrial reaction  
28 kinetics, *in vitro*, *Biophys. J.* 86 (2004) 629-645.  
29  
30  
31  
32  
33  
34  
35  
36  
37  
38  
39  
40  
41  
42  
43  
44  
45  
46  
47  
48  
49  
50  
51  
52  
53  
54  
55  
56  
57  
58  
59  
60